PERGAMON

International Journal of Solids and Structures 38 (2001) 7297–7318

INTERNATIONAL JOURNAL OF SOLIDS and STRUCTURES

www.elsevier.com/locate/ijsolstr

Mechanical aspects of corrosion fatigue and stress corrosion cracking

V.V. Bolotin [a,*], A.A. Shipkov [b]

[a] *Institute of Mechanical Engineering Research, Russian Academy of Sciences, M. Kharitonyevsky per. 4, 101830 Moscow, Centre, Russian Federation*

[b] *Moscow Power Engineering Institute/Technical University, Krasnokazarmennaya Strasse 14, 111250 Moscow, Russian Federation*

Received 19 May 1999

Abstract

The theory of fatigue crack growth based on the synthesis of fracture mechanics and continuum damage mechanics is applied to the prediction of crack growth under cyclic and/or sustained loading in the presence of the aggressive environment. Several aspects of corrosion fatigue and stress corrosion cracking are discussed from the viewpoint of mechanics: the interaction between the damage produced by mechanical and nonmechanical actions and its effect on the fatigue crack propagation; the prediction of the behavior of cracks which shape and size are given more than by a single parameter such as the crack depth; the transfer of the agent within a crack affected by the crack growth and crack "breathing" under cyclic loading. The final results are presented in the form of diagrams illustrating the history of crack sizes, damage measures, stress concentration factors near the tips, and the crack growth rates in function of the principal load and environment parameters.

Keywords: Fracture; Fatigue; Corrosion; Damage; Crack

1. Introduction

The natural environment factors such as moist air, natural water, etc. as well as the substances used in industry, frequently intensify the process of fatigue crack growth. Chemical compositions, concentrations, electro-chemical conditions and temperature are among the most important factors in corrosion fatigue along with the parameters of mechanical cyclic loading. A similar situation takes place under sustained or slowly varying loading when one says on the stress corrosion cracking. A number of other phenomena are related to corrosion fatigue and stress corrosion cracking. Many gaseous media, both natural and used in industry, exhibit a significant influence on fracture and fatigue toughness. A typical case is the hydrogen embrittlement in metals and metallic alloys. A similar effect is produced by intensive irradiation.

* Corresponding author. Fax: +7-95-362-8938.

E-mail addresses: vbolotin@gravity.math.msu.su (V.V. Bolotin), dynamics@deans.mpei.ac.ru (A.A. Shipkov).

0020-7683/01/$ - see front matter
PII: S0020-7683(01)00002-6

Corrosion, aging and embrittlement are the subjects of material science and electro-chemistry. There is the vast literature on corrosion, corrosion fatigue, and stress corrosion cracking (Crooker and Leis, 1983). Most of publications such as the books by Logan (1967), McEvily (1990) and Pokhmursky (1985), deal with experiments and their interpretation in terms of material science and electro-chemistry. As to the numerical prediction of environmentally assisted crack growth, it is based, as a rule, on the superposition principle for crack growth rates or on the slight modifications of this principle (Wei and Gao, 1983; Krausz and Krausz, 1985; Petit et al., 1994). There are only a few publications treating these phenomena from the viewpoint of mechanics (Cherepanov, 1979; Suresh and Ritchie, 1981; Romaniv and Nikiforchin, 1986).

The objective of this paper is to treat corrosion fatigue and stress corrosion cracking from the viewpoint of solid mechanics. Certainly, this approach is one-sided one. Its drawback is that many nonmechanical features will be taken into account in a purely phenomenological way, and some of them will be neglected. However, a similar reproach may be addressed to the common analysis when one neglects many features of mechanical nature or discusses them in a superficial manner.

The presented analysis is based on the synthesis of fracture mechanics and continuum damage mechanics. The leading idea, which has been used in the earlier publications by Bolotin (1983, 1985) in application to ordinary fatigue, is as follows. Crack propagation is considered as a result of interaction between the global balance of forces and energy in the system cracked body – loading (which is the subject of fracture mechanics) and the process of dispersed damage accumulation (which is the subject of damage mechanics). The damage is considered irrespectively to the origin and special features of damage. Staying within a pure phenomenological approach to damage similar to that of continuum damage mechanics (Rabotnov, 1979; Kachanov, 1986), we describe damage by means of continuous functions of coordinates and time. Compared with the analysis of ordinary fatigue cracks, we include nonmechanical types of damage such as chemical, electrochemical, radiation or biological ones. For each type of damage we introduce a special damage measure and the kinetic equation governing their evolution in time. Concentrations, fluxes, and temperature enter these equations as control parameters similar to external stresses and load frequencies in the equations of mechanical damage accumulation. However, there is no sufficient experimental data concerning kinetics of nonmechanical damage accumulation. Therefore, ad hoc phenomenological assumptions are unavoidable, moreover than we do not intend to go into intrinsic subjects of material science.

There are some complications even when we are staying in the framework of mechanics. The main factor controlling corrosion damage near the crack tip is, evidently, the concentration of the aggressive agent at the tip. Since the ''applied'' concentration is given at the crack entrance, the problem arises of the mass transport within the crack hollow. The tip propagates in time, and this propagation is accompanied by intermittent blunting and sharpening. Both diffusion and hydrodynamic mechanisms ought to be included into consideration to assess the conditions within growing fatigue cracks. The crack opening displacements are subjected to cyclic variation including crack closure on the part of the crack length. It means that the mass transport within the crack is an essentially nonstationary process. Thus, the modeling of the environmentally assisted crack propagation, along with the means of fracture and damage mechanics, involves though in a rather limited scope, the means of hydrodynamics.

The structure of this paper is as follows. First, we develop the general theory of fatigue crack propagation which primary sketch was given in the paper by Bolotin (1983), and the developed version in the books by Bolotin (1989, 1998). Then the kinetic equations of damage accumulation are discussed based on the models of continuum damage mechanics. One of the central part of the paper is the discussion of the mass transfer within cracks. Compared with the earlier publications (Bolotin, 1987; Bolotin and Shipkov, 1998), the present analysis is based on the diffusion equation generalized on the case when chemical reactions are present on the crack surfaces, and the crack tip is propagating. Comparison of the numerical results based on the diffusion model and on the simplified phenomenological equation is performed, and the parameters entering the latter equation are assessed. Then the stress corrosion cracks are considered with

the special attention to the interaction between mechanical and corrosion damage, to the influence of the entrance concentration and the crack length on the accumulated damage and the crack growth rate. In the case of corrosion fatigue, the load frequency effects are studied in more detail to separate, as well as possible, the pumping effect of "breathing" cracks, from the effects of entering two temporal variables, natural time and load cycle number.

2. Mechanics of crack growth

A cracked body under loading and environmental action is a special kind of mechanical system. There are two groups of generalized coordinates describing the current state of this system. One group consists of the common Lagrangian coordinates, say, describes the displacements field in the body. Another group of generalized coordinates describes the shape, size and position of cracks. In the paper by Bolotin (1983) we proposed to name these coordinates in honor of A. Griffith, Griffithian generalized coordinates. Later on, for brevity, we say on the *L*-coordinates and the *G*-coordinates, respectively.

Fatigue cracks in solids are usually irreversible. Then the *G*-coordinates, noted $a_1, a_2, \ldots, a_m$ may be chosen in such a way that their variations (named, for brevity, the *G*-variations, see Fig. 1) become non-negative: $\delta a_1 \geqslant 0, \ldots, \delta a_m \geqslant 0$. Discussing fracture and fatigue problems, we split them in two parts, one part dedicated to the evaluation of stress, strain, and displacement fields in the body, and another part dealing with the *G*-coordinates only.

It is expedient, discussing fracture and fatigue problems, to split them in two parts, one dedicated to the evaluation of stress, strain and displacement fields in a body, and one dealing with the *G*-coordinates only. In particular, when quasistatic crack propagation is considered and a variation approach is applied, the states are compared which satisfy all equations of equilibrium, compatibility, etc., as well all boundary conditions. The only generalized coordinates which are subjected to variation are the *G*-coordinates. This means that, studying fracture and fatigue, we deal with mechanical systems with unilateral constraints since all the usual requirements of equilibrium are already satisfied (both in the considered and in neighboring, perturbed states).

Let us consider the quasistatic processes only neglecting all the inertia effects. Assume that the first part of the problem, namely, the evaluation of the *L*-coordinates, is already solved. We consider the system

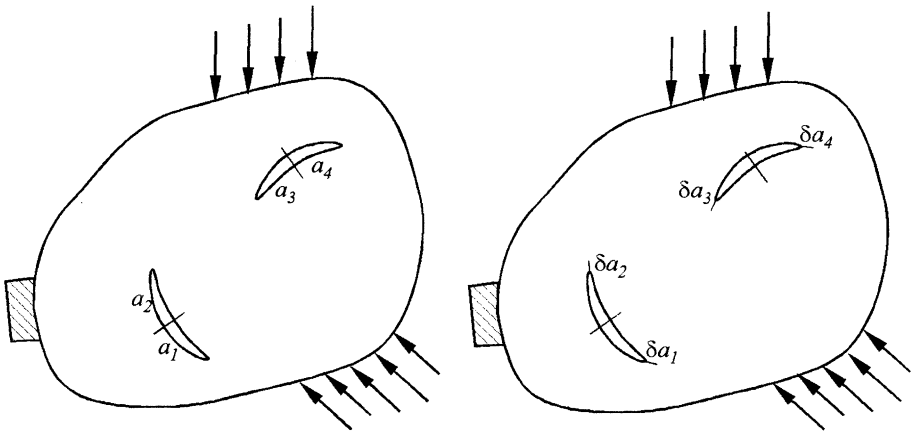

Fig. 1. To the definition of *G*-variations.

cracked body – loading – environment or cracked body – loading device – environment as a mechanical system. The principle of virtual work for this system requires that in equilibrium the conditions hold:

$$\delta_G W \leqslant 0 \tag{1}$$

Here $\delta_G W$ is the virtual work performed with respect to the G-variations, i.e. corresponds to two neighboring states of the body (Fig. 1). Both are the equilibrium states in the ordinary sense but differ in crack dimensions. Depending on the sign in Eq. (1), the state of the body may be stable or unstable with respect to the further crack propagation (Bolotin, 1996). The cracks do not propagate at $\delta_G W > 0$ for all the G-coordinates. Then we say that the system is in a sub-equilibrium state with respect to the G-coordinates. If $\delta_G W < 0$ even for one of the G-coordinates, the state of the system is unstable, and we name this state non-equilibrium. The case $\delta_G W = 0$ named the equilibrium state is of the most importance in the theory of fatigue. This case is typical for slow, stable crack propagation. A crack propagates slowly with respect to a certain G-coordinate at $\delta_G W = 0$, $\delta_G(\delta_G W) < 0$ where the second variation is taken with respect to this coordinate. For other G-coordinates the condition $\delta_G W < 0$ is to be satisfied.

Let this approach to be formulated in terms of generalized forces. The virtual work can be presented as follows

$$\delta_G W = \sum_{j=1}^{m} G_j \delta a_j - \sum_{j=1}^{m} \Gamma_j \delta a_j \tag{2}$$

where δa_j are the variations of the G-coordinates $a_j, \ldots, a_m$; G_j and Γ_j are the generalized forces. All factors driving cracks ahead are referred to the first sum in Eq. (2) where $G_j, \ldots, G_m$ are the generalized driving forces. The resistance to fracture is referred to the second sum, where $\Gamma_j, \ldots, \Gamma_m$ are the generalized resistance forces. The border between the generalized forces G_j and Γ_j is not distinctly defined, especially when the bulk of a body is deformed nonelastically. However, there is the tradition even in the classical fracture mechanics. When we deal with the J-integrals, we distinguish J and J_C; dealing with the strain energy release rates, we distinguish G and G_C.

A subequilibrium state takes place at

$$G_j < \Gamma_j, \quad j = 1, \ldots, m \tag{3}$$

An equilibrium state with respect to the G-coordinates $a_1, \ldots, a_\mu$ takes place at

$$\begin{aligned} &G_j = \Gamma_j, \quad j = 1, \ldots, \mu \\ &G_k < \Gamma_k, \quad k = \mu + 1, \ldots, m \end{aligned} \tag{4}$$

This state is stable when the quadratic form

$$\delta_G(\delta_G W) = \sum_{j=1}^{m} \sum_{k=1}^{m} \frac{\partial H_j}{\partial a_k} \partial a_j \partial a_k \tag{5}$$

is definitely negative in the first ortant of the space $a_j, \ldots, a_\mu$. The notation

$$H_j \equiv G_j - \Gamma_j \tag{6}$$

for the differences of generalized forces is used in Eq. (4).

Eqs. (1)–(5) are valid for modeling the crack growth and final fracture under cyclic and sustained loading including those under the influence of environmental factors such as corrosion and hydrogen embrittlement. However, additional variables ought to be included into consideration to take into account damage both at the crack tips and in the far field, and the change of the geometry of the crack tips.

In modeling fatigue damage, we follow the continuum damage mechanics (Bažant, 1986; Krajcinovic, 1996). The current damage field $\omega(x, t)$ (scalar or tensorial) is a result of loading, environment, and crack growth histories:

$$\omega(x,t) = \overset{\tau=t}{\underset{\tau=t_0}{\Omega}}[s(\tau), a(\tau)] \tag{7}$$

Here x is the spatial coordinate or the reference vector, and t is time. The right-hand side of Eq. (7) is a hereditary functional of loading and environment histories and the crack growth process. These histories are denoted $s(t)$ and $a(t)$, respectively. Another set of variables characterizes the conditions at the crack tips, such as the sizes of process zones and stress concentration in these zones. As in the book by Bolotin (1996), we introduce a set of variables which we name effective tip radii. Their set is governed by a hereditary functional equation such as

$$\rho(t) = \overset{\tau=t}{\underset{\tau=t_0}{R}}[s(\tau), a(\tau), \psi(\tau)] \tag{8}$$

In addition to the variables entering Eq. (7), the tip damage variable $\psi(t)$ is introduced in Eq. (8). This variable may be identified with the set of magnitudes $\omega(x,t)$ at the crack tips.

In fatigue and related phenomena, the generalized forces entering Eqs. (1)–(5) depend not only on $s(t)$, $a(t)$ (that takes place in ordinary fracture mechanics), but on $\psi(t)$ and $\rho(t)$. In particular, the condition of fatigue crack nonpropagation with respect to the G-coordinate a_j within the Nth cycle $t \in (t_{N-1}, t_N]$ is as follows:

$$H_j(N) < 0 \tag{9}$$

Here H_j is the upper band of the difference (6) of the generalized forces

$$H_j(N) = \max_{t_{N-1} \leqslant t \leqslant t_N} \{G_j[s(t), a(t), \psi(t), \rho(t)] - \Gamma_j[s(t), a(t), \psi(t), \rho(t)]\} \tag{10}$$

Similarly, the cracks propagate slowly with respect to the G-coordinates $a_j, \ldots, a_\mu$ at

$$\begin{aligned} &H_j(N) = 0 \quad (j = 1, \ldots, \mu), \qquad H_j(N) < 0 \quad (j = \mu+1, \ldots, m) \\ &\sum_{j=1}^{\mu}\sum_{k=1}^{\mu} \frac{\partial^2 H_j(N)}{\partial a_j \partial a_k} \delta a_j \delta a_k < 0 \end{aligned} \tag{11}$$

As it was shown by Bolotin (1996), the jump-wise crack propagation is also covered by this theory. In this case, the crack growth is presented as a sequence of transitions from one sub-equilibrium state to another one divided by a dimension of the order of the cyclic process zone length. This situation is typical for the low-cycle fatigue. The final fracture with respect to the G-coordinate a_k occurs at

$$H_k(N) > 0 \tag{12}$$

In slowly varying, sustained loading Eqs. (9)–(12) are to be reformulated with the terms of current time t. For example, the condition of crack nonpropagation has the form

$$H_j(t) = G_j[s(t), a(t), \psi(t), \rho(t)] - \Gamma_j[s(t), a(t), \psi(t), \rho(t)] < 0 \tag{13}$$

3. Mass transport within cracks

The environmentally assisted fracture and fatigue are essentially controlled by the transport of the active agent from the crack mouth to the crack tip. The mass transport is a combination of several processes. First, it is the diffusion due to the concentration gradient along the crack. Second, it is the ion migration, which is controlled by electro-chemical potential(s). In the third, purely hydrodynamic processes may be of significance. Even in stress corrosion cracking, when the crack hollow volume is varying in time slowly and monotonically, the convection effects the active agent's transport to the tip. When a crack is short enough

and the cracked surface is in the contact with an intensive outside flow, an additional movement within short cracks may be maintained.

The environment media, both gaseous or liquid, are assumed incompressive, and the term "fluid" is used in both cases. We assume later that a single active agent is present (say, sulfur oxide in air) to avoid two- and multi-phase flow models. Concentrations of the aggressive agents are usually small enough. Then, not to deal with small magnitudes of concentrations, we normalize them relating to a certain standard concentration. For example, for a definite environmental conditions, the concentration may be normalized with respect to that in the external, "fresh" environment. Then the normalized concentration varies as $0 \leqslant c \leqslant 1$. Other variables similar to concentrations will be also normalized. To avoid misunderstandings, we refer to the normalized concentrations as to the agent's contents or just the contents.

Let us consider the simplest case when electro-chemical effects are absent or negligible. It takes place, in particular, when the fluid is nonconductive, or the solid is dielectric. In addition, let the temperature remain constant during the cracking process, and the pressure effect is not significant. Then the mass transfer within a crack is governed by fluid flow and diffusion. The term diffusion is used here in a conditional sense. Saying on diffusion, we mean all the mass transfer mechanisms but fluid flow, i.e. we include the effects of concentration, chemical and electro-chemical potential gradients (Bennet and Myers, 1962). The crack opening displacements are small compared with the crack length. Hence, we may consider the process within a crack as one-dimensional (in two-dimensional fracture problems) or as two-dimensional (in three-dimensional problems). In fact, the content and velocity distribution across the crack hollow may be approximated as uniform, following the planar cross-section distribution or, say, parabolic. This means that the diffusion and the flow are directed along x-axis from the crack entrance at $x = 0$ to the crack front $x = x_t(y)$, Fig. 2(a). Even in three-dimensional problems one may neglect the mass transfer across the crack's hollow presenting all processes as locally one-dimensional.

Under the listed simplification, the equation of agent's transport into the crack depth takes the form

$$\frac{\partial(hc)}{\partial t} + v\frac{\partial(hc)}{\partial x} = \frac{\partial}{\partial x}\left(hD\frac{\partial c}{\partial x}\right) + 2kf(c) \tag{14}$$

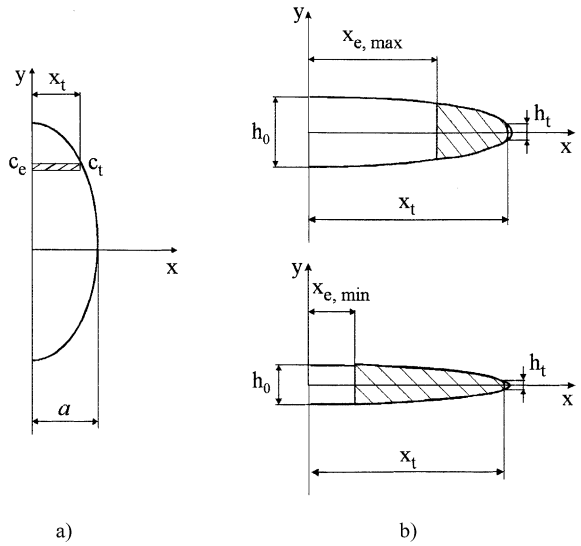

Fig. 2. (a) A near-surface crack in ambient fluid; (b) the pumping effect in cyclic loading.

Here v is the fluid velocity in the x-direction at a fixed y-coordinate, D is the diffusion coefficient, h is the crack opening displacement which we treat as varying along the crack depth. The last term in Eq. (14) takes into account the mass transfer through the crack faces. The corresponding boundary condition has the form

$$\frac{\partial c}{\partial n} = kf(c) \tag{15}$$

with the mass transfer coefficient k. For example, in the case of the first-order reaction we have

$$f(c) = c_s - c \tag{16}$$

Here c_s is some threshold content corresponding to an equilibrium or saturation state. If the mass transfer through the crack surface is modeled as a diffusion in solid phase, the estimate holds $k \sim \lambda(D_s/D)$ with the diffusion coefficient D_s and a characteristic corrosion film thickness λ.

In general, the diffusion coefficient D in Eq. (14) depends on the velocity v (as in the case of turbulent mixing). The mass transfer coefficient k in Eqs. (14) and (15) and, perhaps, the threshold content c_s in Eq. (16) depend on the current corrosion damage. This effect will be taken into account in the further numerical analysis.

To evaluate v, the equations of fluid dynamics have to be used. However, when the fluid is incompressible and the flow is close to one-dimensional, the use of the mass conservation law is sufficient. Actually, the average flow velocity in the x-direction is equal to the stream through the cross-section $x =$ constant divided to the area of this section. Thus, for a planar crack, neglecting the mass transfer through the crack faces, we obtain

$$v(x,y,t) = \frac{1}{h(x,y,t)} \frac{\partial}{\partial t} \left(\int_x^{x_t(y,t)} h(\xi,y,t)\,\mathrm{d}\xi \right) \tag{17}$$

The boundary conditions for Eq. (14) are

$$c = c_e \quad \text{at } x = x_e, \qquad D\frac{\partial c}{\partial x} = kf(c) \quad \text{at } x = x_t \tag{18}$$

where c_e is the agent's content in the "fresh" fluid. The function $kf(c)$, in general, differs from that in Eq. (14). The coordinate x_e corresponds to the cross-section where the fluid may be assumed as "fresh". In stress corrosion cracking, when a crack propagates slowly under constant or slowly varying loading, the first condition (18) is to be taken at the crack mouth, i.e. at $x = 0$. For rapidly growing cracks the border $x = x_e$ moves in depth of the crack. For example, when at $t = 0$ a crack is filled with the "fresh" fluid and then the body is subjected to loading, the boundary coordinate x_e is equal to the root of equation

$$\int_{x_e(y,t)}^{x_t(y,t)} h(\xi,y,t)\,\mathrm{d}\xi = \int_0^{x_t(y,0)} h(\xi,y,0)\,\mathrm{d}\xi \tag{19}$$

Here the mass transfer through the crack faces is also neglected.

Under cyclic loading, especially when the frequency is high, the pumping effect of the "breathing" crack becomes significant. In this case Eq. (19) is to be replaced by the following

$$\int_{x_e(y,t)}^{x_t(y,t)} h(\xi,y,t)\,\mathrm{d}\xi = \int_{x_{e,\min}(y,t)}^{x_t(y,t)} h_{\min}(\xi,y,t)\,\mathrm{d}\xi \tag{20}$$

Here $h_{\min}(\xi,y,t)$ is the crack cross-section profile corresponding to the minimal load within a cycle, i.e. to the maximal crack closure, see Fig. 2(b). Eq. (20) is to be applied consequently for each cycle to follow all the history of fluid entering into a crack hollow.

The contribution of each processes into the mass transport depends, in a major degree, on the relationship between the characteristic times of individual processes. Among these times are the characteristic times for diffusion τ_D, for convection τ_a and τ_f (defined for the crack growth rate $\dot{a} \equiv \mathrm{d}a/\mathrm{d}t$ and the loading frequency f, respectively), and for reaction kinetics τ_k.

$$\tau_D = \frac{a^2}{D}, \quad \tau_a = \frac{a}{\dot{a}}, \quad \tau_f = \frac{1}{f}, \quad \tau_k = \frac{a}{k} \tag{21}$$

Here a is a characteristic crack depth. In the general case, a is to be replaced by x_t. Moreover, for propagating cracks the coordinate x_e of the "fresh" fluid boundary may become comparable with the crack depth. Then the size a in Eq. (21) is to be replaced by the length $x_t - x_e$ of the diffusion path.

Some combinations of the times given in Eq. (21) form nondimensional numbers of similitude. Among them is the diffusion Reynolds number $Re_D = va/D$ where $v \sim a$ for stress corrosion cracking and $v \sim fa$ for corrosion fatigue at high load frequencies. When $Re_D \ll 1$, the convective term in Eq. (14) may be omitted. At $Re_D \sim 1$ both mechanisms have to be considered. At $Re_D \gg 1$ the contribution of the diffusion term must be kept in Eq. (14) not to change the type of the boundary problem. However, at higher fluid velocities, the diffusion coefficient is to be considered as a function of v. This allows to take into account, at least in a heuristic manner, the effects of turbulent mixing.

To illustrate the application of Eqs. (14)–(20), let us consider several numerical examples. The mass transfer within a planar crack with the depth a under steady loading is illustrated in Fig. 3. The crack profile is assumed elliptical, and the absorption on the crack faces is neglected. The following numerical data are used: $D = 10^{-8}$ m^2/s, $k = 10^{-5}$ 1/s at the normalized contents $c_e = 1$, $c_s = 0.5$.

Fig. 3(a) corresponds to a nonpropagating crack at $a = 10$ mm. The points situated near the lines 1 and 2 represent the numerical solution of the boundary problem for two different initial conditions. Line 1 corresponds to the case when at $t = 0$ the active media fills all the crack hollow, i.e. $c(x, 0) = c_e$, $0 \leqslant x \leqslant a$. Line 2 corresponds to an initially "dry" crack when $c(x, 0) = 0$, $0 \leqslant x \leqslant a$. The lines tend to merge rather rapidly, and the characteristic time of merging is $\tau_D = a^2/D = 10^2$ s. The case of a growing crack is presented in Fig. 3(b). It is assumed that the tip propagates with a constant rate, $\mathrm{d}a/\mathrm{d}t = 10^{-6}$ m/s. The same notation is used as in Fig. 3(a). In both cases the content at the tip attains the level close to c_e rather rapidly.

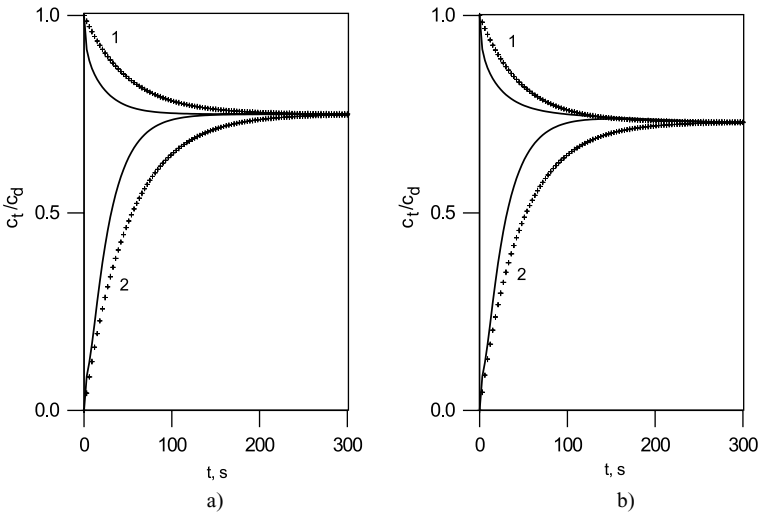

Fig. 3. Agent's content at the tip of the (a) fixed and (b) propagating cracks; lines 1 and 2 are drawn for initially "wet" and "dry" cracks, respectively.

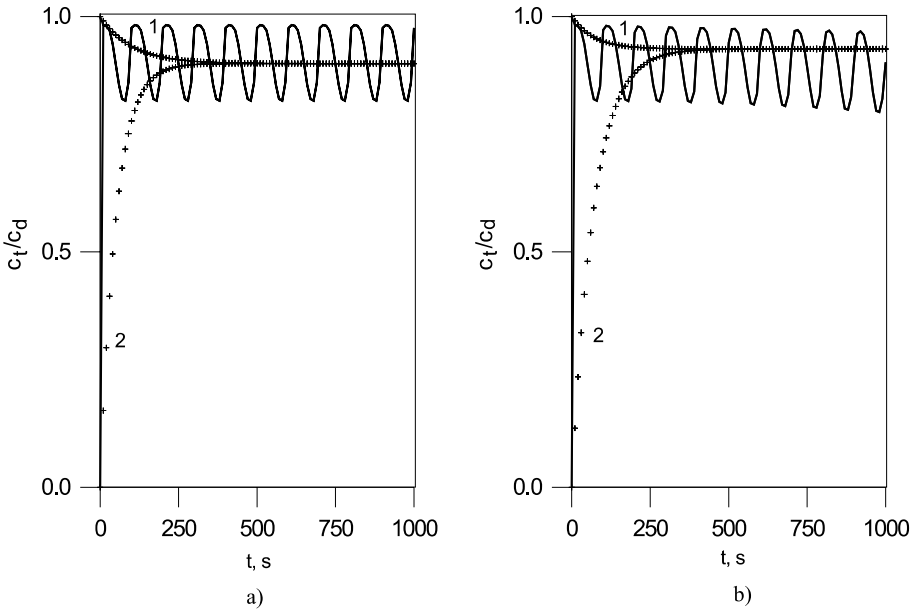

Fig. 4. The effect of crack "breathing" on the agent's content at the tip (notation as in Fig. 3).

Under cyclic loading, the problem is more complex because of the pumping effect. For simplification, let the crack opening displacement be varying in time proportional to the applied stress σ_∞ that is a sinusoidal time function with the frequency f. Then $h_{\min}/h_{\max} = R$ where R is the applied stress ratio, and $h(x,t)$ is also the sinusoidal time function. The same numerical data are used for Fig. 4 as for Fig. 3. In addition, it is assumed that $R = 0.5$, $f = 10^{-2}$ Hz. The latter value corresponds to the characteristic time $\tau_f = 10^2$ s which is on the same order as that of the characteristic diffusion time. Fig. 4(a) is plotted for the fixed crack tip, Fig. 4(b) for the tip moving with the constant rate $\mathrm{d}a/\mathrm{d}t = 10^{-6}$ m/s. The same notation is used as in Fig. 3. The detailed diagram of the initial part is shown in Fig. 5. The qualitative character is the same in all the cases not counting the pumping effect. The fluctuations of the content c_t within a cycle are rather small although the characteristic diffusion time and the cycle duration are on the same order of magnitude. Later on the fluctuations become even smaller. They are also very small for higher load frequencies.

In publications by Bolotin (1998) and Bolotin and Shipkov (1998) a Phenomenological approach to the mass transfer was used. The simplified equation with respect to the tip content c_t was suggested:

$$\frac{\mathrm{d}c_\mathrm{t}}{\mathrm{d}t} = \frac{c_a - c_\mathrm{t}}{\tau_D} + \frac{c_b - c_\mathrm{t}}{\lambda_D}\frac{\mathrm{d}x_t}{\mathrm{d}t} \tag{22}$$

The first term in the right-hand side represents the diffusion mechanism, and the second one the effect of crack propagation. This equation may be interpreted in terms of the material derivatives of $c(x,t)$ at $x = x_t(t)$

$$\frac{\mathrm{d}c_\mathrm{t}}{\mathrm{d}t} = \frac{\partial c_\mathrm{t}}{\partial t} + \frac{\partial c_\mathrm{t}}{\partial x}\frac{\mathrm{d}x_t}{\mathrm{d}t} \tag{23}$$

Comparing Eqs. (14), (18), (22) and (23), one can estimate, at least on the order of magnitude, the parameters c_a, c_b, τ_D and λ_D. In particular, τ_D in Eq. (22) is expected to be close to the characteristic diffusion time in Eq. (21) if we replace a with the length of the diffusion path $x_t - x_\mathrm{e}$. In the presence of the pumping

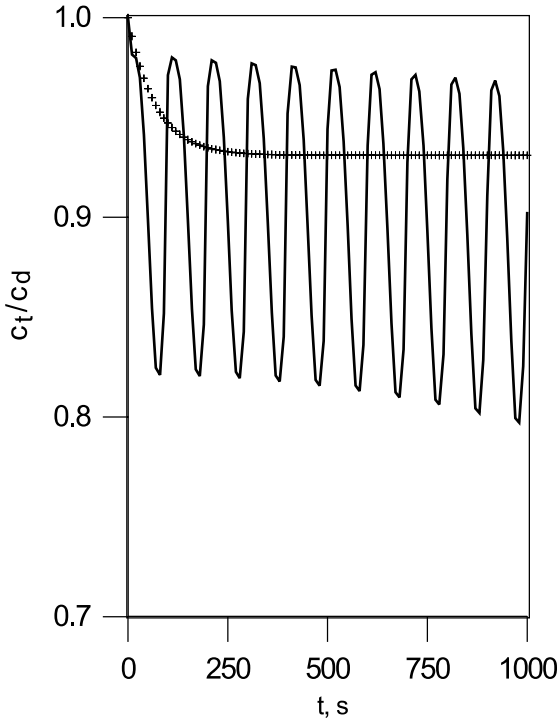

Fig. 5. The detail of the history of the agent's content at the tip.

effect, a certain average length is to be used. The characteristic content c_a is expected to be on the order of the entrance content c_e. The characteristic content c_b and the length parameter λ_D are connected with the mass transfer through the crack tip and, therefore, significantly depend on the current situation near the tip. Probably, c_b is on the order of c_s; following Eq. (18) we obtain the estimate $\lambda_D \sim D/k$. For the data used in the above numerical examples, we have $\tau_D \sim 10^2$ s, $c_a \sim 1$, $c_b \sim 0.5$, $\lambda_D \sim 10^{-3}$ m. The solid lines in Figs. 3 and 4 are drawn according to Eq. (22) accepting these coarse estimates. The agreement of numerical results looks satisfactory.

4. Damage accumulation

To model the process of damage accumulation, we follow the simplest, scalar model of damage ascending to the works by Kachanov (1986) and Rabotnov (1979). They proposed to characterize the dispersed damage with the scalar field $\omega(x,t)$ where $0 \leqslant \omega(x,t) \leqslant 1$. The lower band corresponds to the virgin, nondamaged material, and the upper band to the completely damaged material. Compared with the common scalar approach, we use, instead of a single scalar damage measure, a set of scalar measures. Even when only mechanical actions are considered, it is expedient to distinguish the measures ω_f and ω_s for the damage produced by cyclic and sustained loading, respectively. For the mixed mode cracks, for example kinking and branching cracks (Bolotin, 1989), we distinguish the damage measures corresponding to microcracking in each particular mode. The pure corrosion damage will be described hereafter by a special measure ω_c. If the embrittlement is separately taken into account, the respective measure ω_h also enters into consideration. Thus, the damage field introduced symbolically in Eq. (7) as $\omega(x,t)$, actually consists of a number of scalar damage fields $\omega_1(x,t), \ldots, \omega_v(x,t)$.

Assume that the kinetic equations for particular damage measures are the first-order temporal differential equations. The special case of these equations for mode I cracks is the power-threshold equations such as

$$\frac{\partial\omega_f}{\partial N}=\left(\frac{\Delta\sigma-\Delta\sigma_{\rm th}}{\sigma_f}\right)^{m_f},\qquad \frac{\partial\omega_{\rm s}}{\partial t}=\frac{1}{t_c}\left(\frac{\sigma-\sigma_{\rm th}}{\sigma_{\rm s}}\right)^{m_{\rm s}},\qquad \frac{\partial\omega_c}{\partial t}=\frac{1}{t_c}\left(\frac{c-c_{\rm th}}{c_{\rm d}}\right)^{m_c} \tag{24}$$

Here $\Delta\sigma$ is the range of the opening stress acting in the considered material point, σ is the average or a slowly varying component of this stress, c is the agent concentration in this material point. The expressions in Eq. (24) contain a number of material parameters. Among them parameters σ_f, $\sigma_{\rm s}$ and $c_{\rm d}$ characterize the resistance to damage produced by cyclic loading, sustained loading and ambient agent; $\sigma_{\rm th}$, $\sigma_{\rm th}$ and $c_{\rm th}$ are the corresponding threshold resistance parameters (at $\Delta\sigma<\Delta\sigma_{\rm th}$, $\sigma<\sigma_{\rm th}$, and $c<c_{\rm th}$ the corresponding right-hand sides might be put to zero); the exponents m_f, $m_{\rm s}$, and m_c are, in some aspect, similar to the exponents entering the equations for fatigue and cracks growth rate curves (Bolotin, 1998). The last two expressions in Eq. (24) contain also the time constant t_c. Its magnitude depends on the choice of the material parameters $\sigma_{\rm s}$ and $c_{\rm d}$; otherwise, one may choose t_c arbitrarily, as it is convenient.

The rate of each particular damage measure, in general, implicitly depends on other measures. Actually, the stresses $\Delta\sigma$ and σ depend on the conditions at the crack tip that change due to the damage accumulation of all types. Stress concentration at the tip is given with the effective tip curvature radius ρ. The evolution of ρ is governed by several processes such as crack growth, mechanical damage accumulation, and corrosion. The differential equation for a planar crack with the depth a may be assumed as follows:

$$\frac{{\rm d}\rho}{{\rm d}t}=\frac{\rho_{\rm s}-\rho}{\lambda_a}\frac{{\rm d}a}{{\rm d}t}+(\rho_b-\rho)\frac{{\rm d}(\psi_f+\psi_{\rm s})}{{\rm d}t}+(\rho_c-\rho)\frac{{\rm d}\psi_c}{{\rm d}t} \tag{25}$$

This equation describes the tip sharpening due to the crack growth with the rate ${\rm d}a/{\rm d}t$ till the magnitude $\rho_{\rm s}$, and the tip blunting due to the damage accumulation till the magnitudes ρ_b and ρ_c. Here ψ_f, $\psi_{\rm s}$ and ψ_c are equal to the magnitudes of ω_f, $\omega_{\rm s}$ and ω_c at the tip, λ_a is the parameter with the dimension of length.

There are some complications even in the framework of the comparatively simple Eqs. (24) and (25). The stress range $\Delta\sigma$ and the average stress σ, in general, depend on damage explicitly. For example, let the measures ω_f and $\omega_{\rm s}$ be additive, and the sum $\omega=\omega_f+\omega_{\rm s}$ is interpreted as a measure of microcracking. Then the reduced stress parameters $\Delta\sigma/(1-\omega)$ and $\sigma/(1-\omega)$ are natural to use in Eqs. (24) instead of $\Delta\sigma$ and σ (Vakulenko and Kachanov, 1974). The material parameters in these equations also may vary during the damage accumulation and crack propagation. To take into account the crack closure effect, we must either replace $\Delta\sigma$ with some effective stress range, or treat the material parameters σ_f or $\Delta\sigma_{\rm th}$ or both as functions of the stress ratio. Some secondary effects could be taken into account by generalizing Eq. (24), say, replacing the first equation with the following one ($n_c>0, n_f>0$):

$$\frac{\partial\omega_f}{\partial N}=\left(\frac{\Delta\sigma-\Delta\sigma_{\rm th}}{\sigma_f}\right)^{m_f}\frac{(1-\omega_c)^{n_c}}{(1-\omega_f-\omega_{\rm s})^{n_f}} \tag{26}$$

To evaluate the damage measures, one has to know the current stress–strain and concentration fields in a body during all the process in the consideration. This needs the application of numerical methods. However, there are some approximate approaches. For example, the stress concentration factor κ at the tip of the planar mode I crack and the normal stress distribution on the crack prolongation may be assessed as follows

$$\kappa=1+2Y\left(\frac{a}{\rho}\right)^{1/2},\qquad \sigma=\kappa\sigma_\infty\left[1+\frac{4(x-a)}{\rho}\right]^{-1} \tag{27}$$

The first equation is just an extension of the well-known Neuber's formula upon a broader class of notch geometry taken into account with the form-factor Y. The second equation is the simplest one from the family of empirical equations discussed in the paper by Shin et al. (1994).

As to the distribution of the agent ahead of the tip, we use the fact that the agent penetrates into the solid phase at a comparatively small depth. We refer this depth to the corrosion film thickness λ. This thickness varies during the process of the agent's transport and crack growth. Similar to Eq. (25), it is expedient to assume that the evolution of λ is governed by the first-order differential equation

$$\frac{\mathrm{d}\lambda}{\mathrm{d}t} = \frac{\lambda_\mathrm{s} - \lambda}{\lambda_a} + (\lambda_b - \lambda)\frac{\mathrm{d}(\psi_f + \psi_\mathrm{s})}{\mathrm{d}t} + (\lambda_c - \lambda)\frac{\mathrm{d}\psi_c}{\mathrm{d}t} \tag{28}$$

Here λ_s, λ_b and λ_c are characteristic sizes, and λ_a is the length parameter similar to that in Eq. (25). The first term in the right-hand side describes the thinning of the film because of the crack growth. Other terms take into account the film thickening. In a certain sense, Eq. (28) describes the agent's diffusion through the solid phase under nonstationary conditions. At $\lambda_\mathrm{s} < \lambda_b \leqslant \lambda_c$ the parameter λ_c may be interpreted as the maximal thickness of the corroded film. All these sizes are small compared with the crack length a. As a rule, they are also small compared with the size of the mechanical process zone λ_p, such as the length of the reversed plastic zone in the thin plastic zone model. As the film is very thin, we may use the linear distribution of the concentration $c(x,t)$ within the film thickness $a \leqslant x \leqslant a + \lambda$. Then the agent's distribution near the crack tip will be given with two variables, the tip concentration c_t and the film thickness λ.

The influence of damage on macroscopic, overall material properties is also significant. This influence was extensively studied in many works on micromechanics, see, e.g. the book by Nemat-Nasser and Hori (1993). The most essential effect for us is the change of the fracture toughness. In the framework of the present study, the fracture toughness is introduced with the specific fracture work γ. When the additiveness of damage measures is acceptable, we may put that

$$\gamma = \gamma_0[1 - \chi(\omega_f + \omega_\mathrm{s} + \omega_c)^\alpha] \tag{29}$$

where γ_0 is the specific fracture work for the nondamaged material; $\alpha \geqslant 1$, $0 < \chi \leqslant 1$. At $\omega_f + \omega_\mathrm{s} + \omega_c = 1$ we have the residual specific fracture work for the completely damaged material, $\gamma = \gamma_0(1 - \chi) \geqslant 0$. Other assumptions are equally applicable, in particular those which take into account the effects of cyclic hardening and crack tip shielding (Bolotin, 1998).

5. Stress corrosion cracking

Consider the damage accumulation and crack growth under sustained loading. Let a near-surface planar mode I crack be in the contact with the ambient environment (Fig. 6). The normalized active agent's concentration near the crack entrance c_e is to be constant. The mechanical loading is given by the applied stress σ_∞ and the stress ratio R. The material is linear elastic in the whole body except a small process zone and damaged films at the crack faces. The body is in a plane-strain state. The crack depth a is the only G-coordinate in this case. As it was shown by Bolotin and Lebedev (1996), the contribution of damaged domains into the strain energy release rate may be neglected. Thus, we use for the generalized driving force the Irwin equation

$$G = \frac{K^2(1 - \nu^2)}{E} \tag{30}$$

Here E is Young's modulus, ν is Poisson's ratio, K is the stress intensity factor. As usually, $K = Y\sigma_\infty(\pi a)^{1/2}$ where the geometry factor Y is on the order of unity. For a semi-infinite body $Y = 1.12$.

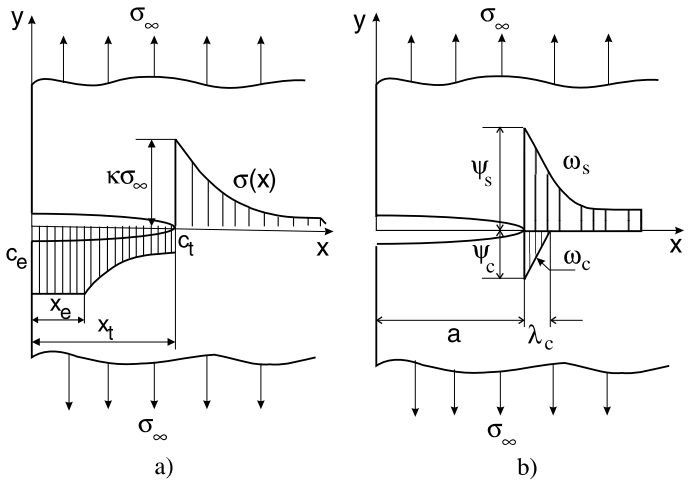

Fig. 6. A near-surface mode I crack: (a) agent's content and tensile stress distribution; (b) mechanical and corrosion damage distribution.

The generalized resistance force, according to Eq. (29), is taken as follows

$$\Gamma = \gamma_0[1 - \chi(\psi_s + \psi_c)^{\alpha}] \tag{31}$$

The same notation as in Eq. (29) is used here except for the damage measures: the tip damage measures ψ_s and ψ_c enter Eq. (31) similar to Eqs. (25) and (28).

The kinetic equations of damage accumulation are given in Eq. (24). We use them in the form (Bolotin, 1989, 1998)

$$\frac{\partial \omega_s}{\partial t} = \frac{1}{t_c}\left(\frac{\sigma - \sigma_{th}}{\sigma_s}\right)^{m_s}, \qquad \frac{d\psi_c}{dt} = \frac{1}{t_c}\left(\frac{c_t - c_{th}}{c_d}\right)^{m_c} \tag{32}$$

Compared with Eq. (24), we introduce here the tip corrosion damage that is governed by the tip content c_t. Within the corrosion film we may assume the corrosion damage measure varying linearly, and being equal to zero outside this film (Fig. 6).

The conditions near the crack tip are described by Eqs. (25) and (28). Not to multiple difficulties, we assume that the film thickness λ is on the same order of magnitude as the effective radius ρ. In any case, in the absence of reliable experimental data, we may treat the similarly positioned material parameters in Eqs. (25) and (28) as equal. The initial conditions, however, may differ significantly. For example, $\rho(0)$ is equal to the initial notch radius, meantime for an initially nondamaged material $\lambda(0) = 0$. Hereafter the equation

$$\frac{d\rho}{dt} = \frac{\rho_s - \rho}{\lambda_a}\frac{da}{dt} + (\rho_b - \rho)\frac{d(\psi_s + \psi_c)}{dt} \tag{33}$$

is used. According to these equations, the tip blunting until the effective radius ρ_b is controlled by the summed damage.

The details concerning the mass transfer problem were discussed in the previous section. We use Eq. (14), the boundary conditions (18) and the linear kinetic Eq. (15). To take into account the effect of damage on kinetics, we have to treat the rate parameter k in Eq. (16), or the saturation content c_s, or both as functions of the corrosion damage measure. Hereafter we take Eq. (15) as

$$\frac{\partial c}{\partial t} = k_0(1-\omega_c^2)(c_s - c) \tag{34}$$

with two constants, k_0 and c_s. In this form the rate $\partial c/\partial t$ enters Eq. (14). As to the second boundary condition (18), we replace $kf(c)$ with $k_0(1-\psi_c)(c_s-c)$ evidently, the current damage on the crack faces is a wake of the tip damage attained in the past.

Eqs. (17) and (19) contain the crack profile function $h(x,t)$. The real profiles are irregular and far from those theoretically predicted in fracture mechanics, linear or nonlinear. A real crack certainly becomes wider when we go from the tip to the entrance. An elementary dimension analysis gives

$$h_0 = \frac{4Z_0\sigma_\infty a(1-\nu^2)}{E}, \quad h_t = \frac{Z_t\sigma_\infty^2 a}{E\sigma_Y} \tag{35}$$

where σ_Y is the yield stress or its equivalent. The coefficients Z_0 and Z_t are on the order of unity. They have to be chosen to achieve the agreement with the experimental data or with the theoretical predictions of fracture mechanics (Kanninen and Popelar, 1987; Wnuk, 1990). In particular, the estimate $Z_0 = 1.458$ is mentioned in the literature.

The shape of the edge crack profile was widely discussed in the literature in connection with the method of estimating of the tip opening displacement at the crack entrance (Matsoukas et al., 1984; Raju et al., 1992). Linear, parabolic, and elliptical profiles were compared. No closed form solutions are known for the edge cracks in nonlinear fracture mechanics; the available solution in the framework of the plastic zone model was obtained by a numerical analysis approach (Fenner, 1974; Petroski, 1979; Atluri, 1986). On the other side, modeling of cracks as truncated hollows with the tip cross-section size h_t seems contradictory when the analysis is performed for a linear elastic material. An attempt to treat corrosion fatigue using the thin plastic zone model was performed by Bolotin et al. (1998). In this study, the magnitude 2ρ cannot be interpreted as h_t because ρ is not a geometry parameter but the characteristics of stress concentration near the damaged tip. As it follows from Eq. (35), $h_0/a \sim \sigma_\infty/E$, $\quad h_t/h_0 \sim \sigma_\infty/\sigma_Y$, i.e. the crack hollow is very narrow. As a result, all the three profiles give rather close results. Hereafter we assume the elliptical profile with the semi-axes $a[1-(h_t/h_0)] \approx a$ and $(1/2)h_0$.

The following numerical data are used in the following examples. Material properties are $E = 200$ GPa, $\nu = 0.3$, $\sigma_s = 5$ GPa, $\sigma_{th} = 250$ MPa, $c_{th} = 0$, $m_s = m_c = 4$, $t_c = 10^6$ s, $\gamma_0 = 10$ kJ/m^2, $\alpha = \chi = 1$. In Eq. (31) we assume that $\rho_s = 10$ μm, $\rho_b = \lambda_a = 100$ μm. The parameters of the mass transfer are $D = 10^{-8}$ m^2/s, $k_0 = 10^{-5}$ m/s, $c_s/c_d = 0.5$. The agent's concentration at the crack entrance is given by the ratio c_e/c_d. The applied stress σ_∞ and the entrance content c_e are kept constant during all the crack history including the initiation stage. The stress distribution ahead of the tip is taken according to Eq. (27). The material is considered as initially nondamaged, i.e. $\omega_s = \omega_c$ at all x. The initial crack size is $a_0 = 1$ mm, the initial effective crack radius $\rho_0 = 50$ μm. The crack is initially "wet", i.e. its hollow is initially filled by the "fresh" fluid.

The computational procedure is rather complicated. It consists of a number of sub-procedures with feedbacks which require the corresponding iterations. During the initiation stage, the generalized forces G and Γ satisfy the condition $G < \Gamma$. The crack growth starts at the first attainment the equality $G = \Gamma$. The further crack propagation occurs at $G = \Gamma$ until the final fracture. To estimate the damage measures ψ_s and ψ_c, the expressions in Eq. (32) have to be integrated that requires evaluating of the current opening stress σ and the tip agent's content c_t. The first variable is computed using the approximate formulae (27) accompanied with integrating Eq. (33). The second variable is determined from the solution of the mass transfer problem. It is obvious that all these calculations are multiconnected and jointly conditioned. Some details concerning the organization of the numerical procedures in fatigue problems can be found in the book by Bolotin (1998).

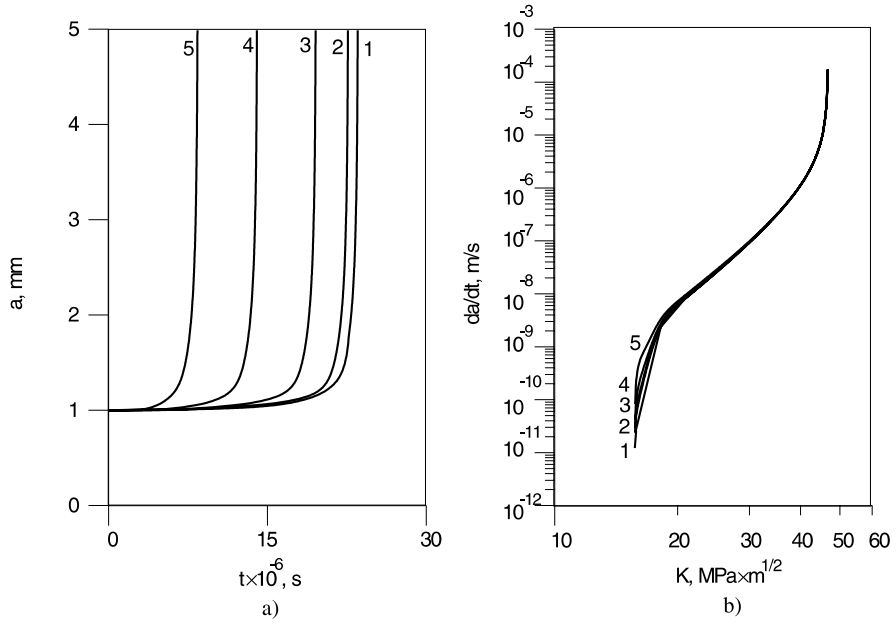

Fig. 7. Crack growth in stress corrosion cracking: (a) crack length histories; (b) crack growth rate diagrams; lines 1, 2, 3, 4, and 5 are drawn for $c_e/c_d = 0$, 0.25, 0.5, 0.75, and 1.

The crack growth histories are illustrated in Fig. 7 which is obtained for $\sigma_\infty = 100$ MPa, $c_e/c_d = 0$, 0.25, 0.5, 0.75, and 1 (lines 1, 2, 3, 4, and 5, respectively). Fig. 7(a) presents the crack depth a in function of time t, Fig. 7(b) presents the rate da/dt in function of the stress intensity factor K. The crack growth rate diagrams presented in Fig. 7(b) look similar to those observed in experimentation (Nakai, 1994; Petit et al., 1994). Each diagram covers the stage of the initiation and early growth at lower K, and almost linear, in log-log scale, stage which is usually referred to as Paris' stage, and the final stage when a crack is approaching the final fracture. The crack growth rates vary in a large scale for short cracks. In the process of crack growth, the lines, corresponding to various contents tend to merge. Similar to the purely mechanical fatigue, the slope of the Paris' stage line is rather close to the power exponent $m_s = m_c = 4$ in the equations of damage accumulation. This fact was observed in the earlier papers by Bolotin (1983, 1985) on the cyclic fatigue and substantiated by analytical calculation in the so-called "quasistationary approximation" (Bolotin, 1998). At $m_s < m_c$ this conclusion is not valid, although the magnitudes of the Paris' stage exponent from the interval $m_c \leqslant m \leqslant m_s$ are expected.

It is natural that the aggressive environment accelerates the crack growth. There are, however, some qualitative patterns depending on the agent's content. At low content, such as $c_e/c_d = 0.25$, the crack growth rate diagram shown by line 2 in Fig. 7(b) looks similar to that at $c_e/c_d = 0$ (line 1). A comparative weak dependence of the rate da/dt on K is observed when the agent's content is high and the stress intensity factor is low. For example, at $c_e/c_d = 1$ a tendency to the formation of a "plateau" is observable in the beginning of the diagram (line 5). It signifies that the crack growth is mostly controlled by corrosion. Later, the mechanical damage becomes significant that results into increasing of the rate. This pattern is similar to that observed in experiments (Crooker and Leis, 1983; Nakai, 1994).

Fig. 7 exhibits the general features of experimental diagrams. The following diagrams illustrate the phenomena which are of most intrinsic nature and difficult to be observed directly. In Fig. 8(a) the histories of the agent's content at the tip are shown. Compared to Fig. 3 corresponding to artificial conditions,

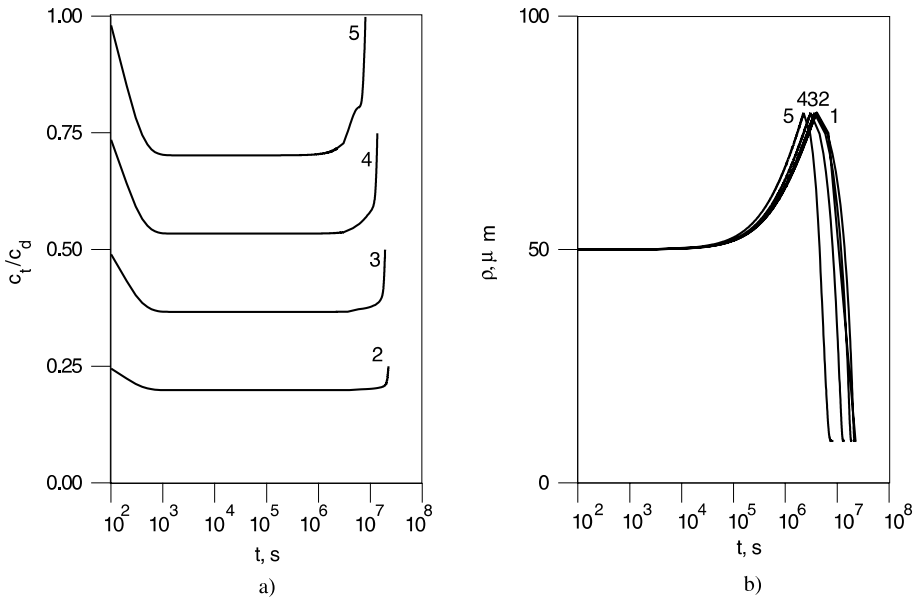

Fig. 8. (a) The agent's content and (b) the effective tip radius in stress corrosion cracking; notation as in Fig. 7.

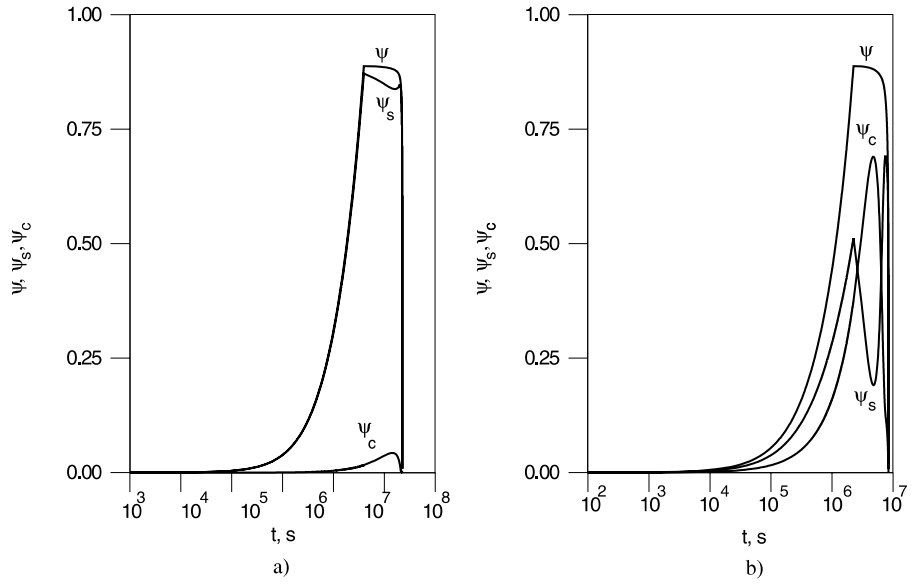

Fig. 9. Mechanical, corrosion, and summed damage measures at the crack tip in stress corrosion cracking: (a) $c_e/c_d = 0.25$; (b) $c_e/c_d = 1$.

Fig. 8(a) is obtained from the joint modeling of the complex process which includes mass transfer, damage accumulation and crack growth. Recall that in this example we consider initially "wet" cracks. When the tip is fixed, the tip content diminishes because of the absorption on the crack surfaces. When the crack begins to grow, the content remains almost constant during the significant section of the fatigue life. The process of mass transfer becomes intensive at higher crack growth rates. As a result, we observe increasing

of the tip content on the later stage of the fatigue life. Close to the final fracture, a large portion of the "fresh" fluid enters the crack hollow resulting into the growth of the tip content. All these patterns are the result of the interaction between several mechanisms of mass transfer in a system with moving boundaries.

Fig. 8(b) shows the tip effective radius histories. At the beginning a monotonous blunting of the tip occurs. This process proceeds until the moment of the crack growth start. Then the tip begins to sharpen. Most of the final stage of the fatigue life, the stress concentration at the tip corresponds to the "sharp" radius ρ_s.

The evolution of damage measures is illustrated in Fig. 9. Fig. 9(a) is plotted for $c_e/c_d = 0.25$, i.e. for a comparatively low concentration of the ambient agent. The mechanical damage measure ψ_s dominates in this case during all the fatigue life. This measure as well as the summed damage measure $\psi = \psi_s + \psi_c$ increase monotonously when the tip is fixed. They both begin to decrease when the tip starts to propagate. The final fracture occurs practically at the zero damage. Fig. 9(b) is plotted for $c_e/c_d = 1$. Contrary to Fig. 9(a), the corrosion damage dominates here during all the fatigue life. As to the mechanical damage, its measure varies in time nonmonotonously. In particular, a significant growth is observed near the final fracture. It is to be noted that the measures ψ_s, ψ_c and ψ relate to material particles located at the crack tip. This means that, beginning from the crack growth start, these variables have to be referred to different material particles.

6. Corrosion fatigue

The modeling of corrosion fatigue is more complex because of the essential nonstationarity of loading and mass transfer processes. The general approach to modeling is based on Eqs. (10), (14), (17), (19), (24), (25), (28), and (29).

Consider, as in the previous section, a planar mode I crack. The applied stress σ_∞ is given as

$$\sigma_\infty(t) = \sigma_{\infty,m} + \frac{1}{2}\Delta\sigma_\infty \sin 2\pi f t \tag{36}$$

with the average stress $\sigma_{\infty,m}$, the stress range $\Delta\sigma_\infty$, and the load frequency f. We assume all these parameters to be constant during all the fatigue life. Obviously, this limitation is not essential in the numerical analysis. We use Eq. (27) to evaluate the stress distribution ahead of the tip, and Eq. (30) for the generalized driving force G. The stress intensity factor in Eq. (30) must be taken at $\sigma_{\infty,\max} = \sigma_{\infty,m} + (1/2)\Delta\sigma_\infty$. Another feature is the involvement of three damage measures, ψ_s, ψ_f, and ψ_c corresponding to the sustained loading, cyclic loading and environmental action, respectively. Thus, instead of Eq. (31) we use the equation

$$\Gamma = \gamma_0[1 - \chi(\psi_s + \psi_f + \psi_c)^\alpha] \tag{37}$$

and instead of Eq. (33) the equation

$$\frac{d\rho}{dt} = \frac{\rho_s - \rho}{\lambda_a}\frac{da}{dt} + (\rho_b - \rho)\frac{d(\psi_s + \psi_f + \psi_c)}{dt} \tag{38}$$

The additiveness of damage measures is assumed in Eqs. (37) and (38); in particular the "blunt" effective radius is referred to the summed damage measure $\psi = \psi_s + \psi_f + \psi_c$.

The computations are performed for the same numerical data as in the previous section with the supplements inherent to cyclic loading. It is assumed that the stress σ_∞ in Eq. (36) is given with the stress range $\Delta\sigma_\infty$ and the stress ratio R, and in all the diagrams $\Delta\sigma_\infty = 150$ MPa, $R = 0.5$. The material parameters in the equation of cyclic damage accumulation are: $\sigma_f = 5$ GPa, $\Delta\sigma_{th} = 125$ MPa, $m_f = 4$. In all the numerical examples except that presented in Fig. 14, the load frequency is $f = 10^{-2}$ Hz.

Because of the unsteady behavior of almost all variables in cyclic loading, the computations are more laborious than in the case of stress corrosion cracking. Rigorously, one has to perform the computations

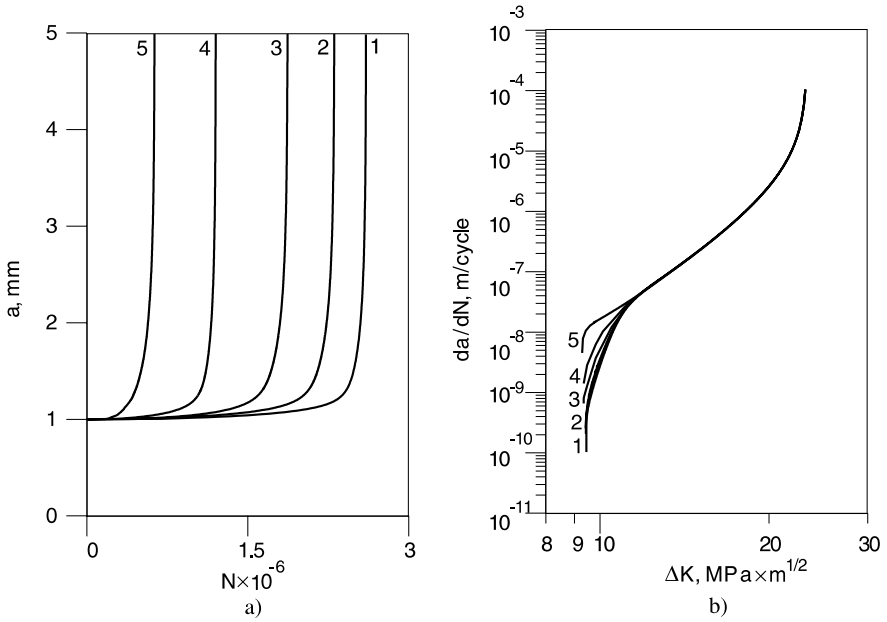

Fig. 10. Crack growth in stress corrosion fatigue: (a) crack length histories; (b) crack growth rate diagrams; lines 1, 2, 3, 4, and 5 are drawn for $c_e/c_d = 0$, 0.25, 0.5, 0.75, and 1.

using the temporal steps on the order of 0.1 of the cycle duration, and even less. This approach is applied on the initial stage of the fatigue life. Since the total fatigue life is measured in hundred thousands and even millions cycles, such a detailed approach consumes too much processor time. On the other side, the range of fluctuations of the agent's content at the tip is small. To simplify the numerical procedure, the averaging of fluctuating variables upon a cycle is applied. Thus, the computations are performed using the blocks of cycles. The checking of equilibrium and stability conditions is performed with respect to maxima of the difference $H(N) = G(N) - \Gamma(N)$ attained within each block.

Fig. 10 illustrates the crack propagation at different agent's content. Lines 1, 2, 3, 4, and 5 are drawn for $c_e/c_d = 0$, 0.25, 0.5, 0.75, and 1. The crack depth histories are plotted in Fig. 10(a), and the crack growth rate diagrams in Fig. 10(b). As usual, the rate is measured in da/dN which is considered as a function of stress intensity factor range $\Delta K = Y\Delta\sigma_\infty(\pi a)^{1/2}$. The general patterns are similar to those in stress corrosion fatigue (Fig. 7). However, there are peculiarities connected with the cyclic loading. Namely, the lines in the crack growth rate diagram exhibit an unsteady behavior, especially on the earlier stage. When the agent's content is high, the early stage of crack growth is primarily controlled by corrosion. To the contrary, the last stage is primarily controlled by cyclic loading. It is distinctly seen in Fig. 10(b) where the lines corresponding to the different variables c_e/c_d tend to merge with the growing range ΔK. The slope of the middle section is close to $m = 4$. Recall that in this numerical example $m_s = m_f = m_c = 4$.

The duration of the initiation stage can be observed in Fig. 11 where the histories $\rho(N)$ of the effective tip radius at various c_e/c_d are presented. The moment of the crack growth start corresponds to the maximums. The concluding stage takes place at the effective tip radius close to $\rho_s = 10$ μm.

Some results concerning the mass transfer process are shown in the Fig. 12. The histories of the tip content are presented in Fig. 12(a). They are obtained at $c_e/c_d = 0$, 0.25, 0.5, 0.75, and 1 (lines 2, 3, 4, and 5). All the lines exhibit unsteadiness, especially when the tips begin to propagate. The main source is certainly the pumping effect and the intermittent change of the boundary condition at the crack tip. Partially this effect may be attributed to the computational procedure that includes the solution of the mass

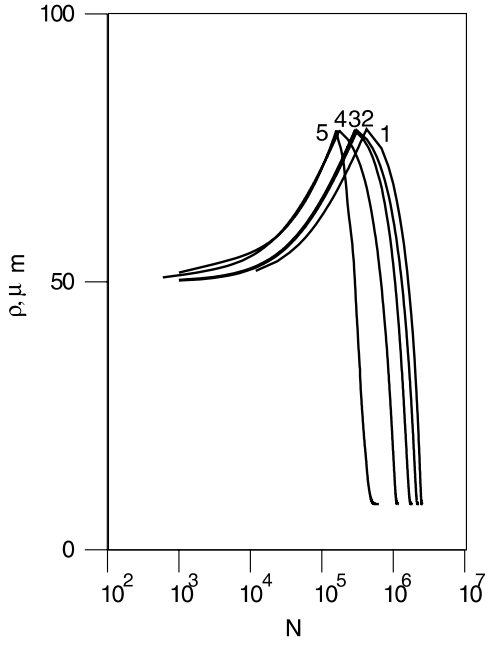

Fig. 11. Effective tip radius in corrosion fatigue (notation as in Fig. 10).

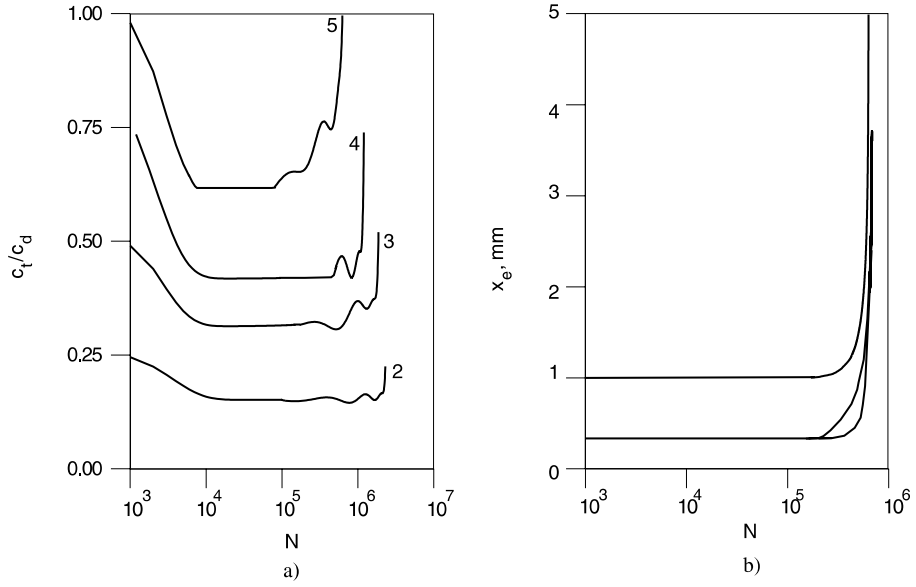

Fig. 12. The mass transport within breathing cracks: (a) agent's content at the tip for $c_e/c_d = 0.25$, 0.5, 0.75, and 1 (lines 1, 2, 3, and 4); (b) maximal (1), average (2) and minimal (3) coordinates of the "fresh" agent's boundary within a cycle at $c_e/c_d = 1$.

transfer problem in steps containing the blocks of cycling loading. It has to be recalled that we consider the nonstationary mass transfer to the moving boundary. This nonstationarity is illustrated in Fig. 12(b) where the range of varying of the border coordinate x_e is shown. The diagram is plotted at $R = 0.5$. Then,

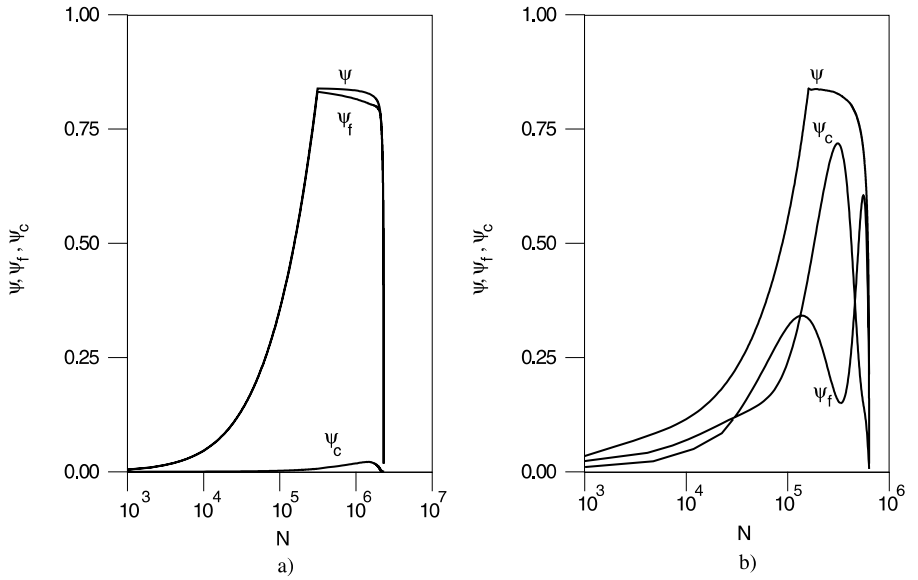

Fig. 13. Mechanical, corrosion, and summed damage measures at the crack tip in corrosion fatigue: (a) $c_e/c_d = 0.25$; (b) $c_e/c_d = 1$.

according to Eqs. (20), (35), and (37), a part of the the "fresh" fluid leaves the crack hollow at $\sigma_\infty = \sigma_{\infty,\min}$ and enters at $\sigma_\infty = \sigma_{\infty,\max}$. When a crack propagates, the amount of the of the "fresh" fluid increases, and the border coordinate x_e approaches the tip coordinate x_t.

The distribution of the summed damage measure $\psi = \psi_s + \psi_f + \psi_c$ between its components is illustrated in Fig. 13. Fig. 13(a) is plotted for $c_e/c_d = 0.25$, Fig. 13(b) for $c_e/c_d = 1$. Similar to the case of stress corrosion cracking, the summed damage grows when the crack tip is fixed, begins to diminish during the crack propagation, and attains very small magnitudes at the moment of final fracture. The contribution of each type of damage depends on the concentration of the agent, the stress ratio, and the relationship between the cycle duration and the characteristic diffusion time. In the considered example, because of the assumed numerical data, the contribution of sustained loading is small compared with that of cyclic loading. The diagrams for partial damage measures exhibit nonstationarities. The corrosion damage sometimes increases even after the start of crack growth. A drop of the mechanical damage occurs simultaneously. In general, a kind of competition between mechanical and corrosion damage is observed in Fig. 13. The summed damage, however, behaves regularly.

The frequency effect is one of the features in corrosion fatigue compared to stress corrosion cracking. Cyclic fatigue proceeds in cycles, corrosion in the natural time units. Several types of crack growth rate diagrams are used for presenting experimental results (McEvily, 1990). The crack growth rates interpreted as $\mathrm{d}a/\mathrm{d}N$ are usually plotted against the range ΔK of the stress intensity factor. When the rates are interpreted as $\mathrm{d}a/\mathrm{d}t$, the maximum or average stress intensity factor, or the agent's concentration are used as control parameters. The load frequency is also one of the important control parameters. The choice depends on dominating mechanisms.

Two families of diagrams are plotted in Fig. 14 for the following numerical data: $\Delta\sigma_\infty = 150$ MPa, $R = 0.5$, $c_e/c_d = 1$, and the load frequencies are $f = 10^{-3}$, 10^{-2}, 10^{-1}, and 1 Hz (lines 1, 2, 3, and 4, respectively). Fig. 14(a) presents $\mathrm{d}a/\mathrm{d}N$ as a function of ΔK, meanwhile Fig. 14(b) shows $\mathrm{d}a/\mathrm{d}t$ as a function of $K_{\max} = \Delta K(1-R)^{-1}$. Note, that the order of lines in Fig. 14(a) and (b) is different. The frequency effect is significant, especially when the crack growth rate is measured in $\mathrm{d}a/\mathrm{d}N$. The difference in $\mathrm{d}a/\mathrm{d}N$ is measured up to three orders of magnitude when the frequency f is changed from 10^{-2} to 10 Hz. The difference in

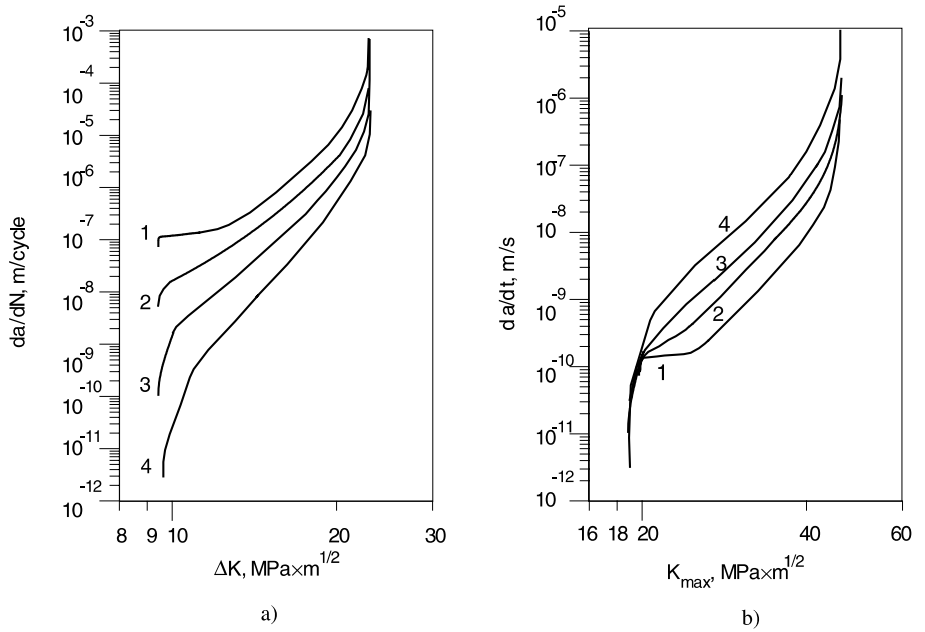

Fig. 14. Frequency effects in corrosion fatigue: crack growth rate measured in da/dN (a) and in da/dt at $f = 10^{-3}$, 10^{-2}, 10^{-1}, and 1 Hz (lines 1, 2, 3, and 4, respectively).

da/dt does not exceed one order of magnitude. When a crack penetrates in depth, the divergence of rates diminishes because of increasing of the mechanical damage contribution. Approaching the final fracture, the role of maximal stresses increases. The final fracture occurs in the vicinity of $\Delta K = K_c(1 - R)$ or $K_{\max} = K_c$, where $K_c \approx (\gamma_0 E)^{1/2}$ is the fracture toughness characteristics for the nondamaged material.

7. Conclusion

The model of crack start and growth under the combination of mechanical and environmental actions was suggested based on the synthesis of fracture mechanics and continuum damage mechanics. Compared with the previous studies, several damage measures were introduced for describing the damage under cyclic and sustained components of loading, as well as the damage as a result of corrosion. The model includes the kinetic equations for the accumulation of each type of damage, the equation describing the evolution of conditions at the moving crack tip, and the equation of mass transfer within the crack. The latter equation and the accompanying boundary conditions take into account the agents' diffusion and related phenomena as well as the fluid flow in a channel of an unsteady geometry. The results of the numerical simulation were presented both for stress corrosion cracking and corrosion fatigue at various agent's contents, various load frequencies, etc. Along with the crack size histories and the crack growth rate diagrams, the diagrams illustrating the evolution of the conditions near the tips were presented. The crack growth rate diagrams exhibit a qualitative agreement with experimental data published in the literature. The quantitative agreement can be achieved by the appropriate choice of material parameters. Some newly introduced variables such as damage measures are difficult to assess in the direct observation. However, the use of these variables offers an additional way for the insight into the mechanical aspects of environmentally assisted damage and fracture.

Acknowledgement

This work was partially supported by the Russian Foundation for Basic Research (grants 99-01-00282 and 00-15-96138).

References

Atluri, S. (Ed.), 1986. Computational Methods in Mechanics of Fracture. North-Holland, Amsterdam.
Bažant, Z.P., 1986. Mechanics of distributed cracking. Applied Mechanics Reviews 39, 675–705.
Bennet, K.O, Myers, J.E., 1962. Momentum, Heat and Mass Transfer. McGraw-Hill, New York.
Bolotin, V.V., 1983. Equations of fatigue crack growth. Izvestiya AN SSSR, Mekhanika Tverdogo Tela, No. 4, pp. 153–160 (in Russian).
Bolotin, V.V., 1985. A unified approach to damage accumulation and fatigue crack growth. Engineering Fracture Mechanics 22, 387–398.
Bolotin, V.V., 1987. Mechanical models of stress corrosion cracking. Mashinovedeniye, no. 4, pp. 20–26 (in Russian).
Bolotin, V.V., 1989. Prediction of Service Life for Machines and Structures. ASME Press, New York (Russian edn. 1984).
Bolotin, V.V., 1996. Stability Problems in Fracture Mechanics. Wiley, New York.
Bolotin, V.V., 1998. Mechanics of Fatigue. CRC Press, Boca Raton, Florida.
Bolotin, V.V., Lebedev, V.N., 1996. Analytical model of fatigue crack growth retardation due to overloading. International Journal of Solids and Structures 33, 1129–1243.
Bolotin, V.V., Shipkov, A.A., 1998. A model of the environmentally affected growth of fatigue cracks. Journal of Applied Mathematics and Mechanics 62, 289–296.
Bolotin, V.V., Kovekh, N.M., Shipkov, A.A., 1998. Modelling of corrosion fatigue crack growth. Problemy Machinostroyeniya i Nadezhnosti Mashin, no. 5, pp. 67–71 (in Russian).
Cherepanov, G.P., 1979. The Mechanics of Brittle Fracture. McGraw-Hill, New York.
Crooker T.W., Leis B.N., 1983. Corrosion Fatigue: Mechanics, Metallurgy, Electrochemistry, and Engineering. ASTM STP 801, ASTM, Philadelphia.
Fenner, N.N., 1974. Dugdale mode solution for a single edge cracked plate. International Journal of Fracture 10, 71–76.
Kachanov, L.M., 1986. Introduction to Continuum Damage Mechanics. Martinus Nijhoff, Dordrecht.
Kanninen, T., Popelar, G., 1987. Advanced Fracture Mechanics. Pergamon Press, Oxford.
Krajcinovic, D., 1996. Damage Mechanics. Elsevier, North-Holland, Amsterdam.
Krausz, A.S., Krausz, K., 1985. Fracture Kinetics of Crack Growth. Kluwer, Dordrecht.
Logan, H.L., 1967. The Stress Corrosion in Metals. Wiley, New York.
Matsoukas, M., Cottrel, B., May, Y.W., 1984. On the plastic rotation constant used in standard COD tests. International Journal of Fracture 26, 49–53.
Nakai, Y., 1994. Fatigue crack propagation in aqueous environment. In: Carpinteri A. (Ed.), Handbook of Fatigue Crack Propagation in Metallic Structures. Elsevier, Amsterdam, 1243–1275.
Nemat-Nasser, S., Hori, M., 1993. Micromechanics: Overall Properties of Heterogeneous Materials. North-Holland, Amsterdam.
Petit, J., de Fouquet, J., Henaff, G., 1994. Influence of ambient atmosphere on fatigue crack growth behaviour of metals. In: Carpinteri, A. (Ed.), Handbook of Fatigue Crack Propagation in Metallic Structures. Elsevier, Amsterdam, pp. 1159–1203.
Petroski, H.J., 1979. Dugdale plastic zone sizes for edge cracks. International Journal of Fracture 15, 217–230.
Pokhmursky, V.Z., 1985. Corrosion Fatigue of Metals. Metallurgiya, Moscow (in Russian).
Rabotnov, Yu.N., 1979. Mechanics of Deformable Solids. Nauka, Moscow (in Russian).
Raju, I.S., Newman, J.C., Atluri, S.N., 1992. Crack-mouth displacements for semi-elliptical surface cracks subjected to remote tension and bending loads. Fracture Mechanics: 22nd Symposium, vol. 2. ASTM STP 1131, ASTM, Philadelphia, pp. 19–28.
Romaniv, O.M., Nikiforchin, G.N., 1986. Mechanics of Corrosion of Structural Alloys. Metallurgiya, Moscow (in Russian).
Shin, C.S., Man, K.C., Wang, C.M., 1994. A practical method to estimate the stress concentration of notches. International Journal of Fatigue 16, 242–256.
Suresh, S., Ritchie, R.O., 1981. Mechanism of environmentally assisted fatigue and growth in low strength steels. In: Francois, D. (Ed.), Advances in Fracture Research, Pergamon Press, Oxford.
Vakulenko, A.A., Kachanov, M.L., 1974. Continuum theory of cracked media. Izvestiya AN SSSR, Mekhanika Tverdogo Tela, No. 4, pp. 159–166 (in Russian).
Wei, R.P., Gao, M., 1983. Reconsideration of the superposition model for environmentally assisted fatigue crack growth. Scripta Metallurgica et Materialia 17, 959–962.
Wnuk, M.P. (Ed.), 1990. Nonlinear Fracture Mechanics. CISM Course 314, Springer-Verlag, Wien-New York.